

# Arrival-Based Equalizer for Underwater Communication Systems

Salman Ijaz, António Silva, Sérgio M. Jesus  
 Laboratório de Robótica e Sistemas em Engenharia e Ciência (LARsys),  
 Campus de Gambelas, Universidade do Algarve,  
 8005-139, Faro, Portugal.  
 Email: {ssiddiqui,asilva,sjesus}@ualg.pt

**Abstract**—One of the challenges in the present underwater acoustic communication systems is to combat the underwater channel effects which results in time and frequency spreading of the transmitted signal. The time spreading is caused by the multipath effect while the frequency spreading is due to the time variability of the underwater channel. The passive Time Reversal (pTR) equalizer has been used in underwater communications because of its time focusing property which minimizes the time spreading effect of the underwater channel. In order to compensate for the frequency spreading effect, an improved version of pTR was proposed, called Frequency shift passive time reversal (FSpTR). FSpTR tries to compensate for the frequency spreading by applying a frequency shift in the estimated channel impulse response (IR). In the multipath environment, multiple replicas of the transmitted signal reaches the receiver through different paths where each path is affected differently by environmental variations. In such cases, a single frequency shift fails to compensate for the environmental variations on each path, resulting in degradation in the performance. In this paper, an arrival-based equalizer is proposed to compensate for the environmental variations on each path. The concept of beamforming is integrated with FSpTR equalizer, in this paper, to compensate each arrival separately for the environmental variations. The proposed equalizer is tested with the real data and the results showed that the proposed approach outperforms pTR and FSpTR equalizers and provides a mean MSE gain of 4.9 dB and 4.2 dB respectively.

**Index Terms**—Underwater Communication, Passive Time Reversal equalizer, Frequency shift passive time reversal equalizer, Geometric variations, Doppler, Beamforming

## I. INTRODUCTION

Underwater acoustic communications is an open field of research which offers great challenges due to adverse environmental effects. Achieving reliable underwater communications is still a great challenge due to strong time varying multipath environment and Doppler spread. Due to these effects the received signal spreads both in the time and frequency making equalization a challenging task. The main idea of this paper is to combine Frequency Shift Passive Time Reversal (FSpTR) technique [1] with beamforming processing to improve the performance of the underwater communication systems.

In the last decade, Time Reversal (TR) communication system has emerged as an effective technique for underwater acoustic communication. The TR communication system offers lower complexity than traditional equalization systems and the

spatial and temporal focusing capability of TR system makes it most favorable for underwater communication applications specially in a multipath environment [2], [3], [4]. In TR communication, the received signal is correlated with the time reversed version of the estimated impulse responses (IR) of the channel. There are two types of time reversal systems, active time reversal (aTR) and passive time reversal (pTR). In this paper, pTR system is considered. In pTR, a single source and a vertical line array (VLA) are used. A probe signal is transmitted ahead of the data for the channel IR estimation. The IR estimate is then used as a synthetic channel for the temporal focusing of the data signal, which is equivalent to the deconvolution of the multipath generated by the real channel.

The time spreading of the underwater channel, which is due to the multipath effect, greatly effects the temporal focusing by inducing intersymbolic interference (ISI), which results in the degradation of the system performance [5], [6]. The standard approach is to design an equalizer that attempts to compensate for the multipath and to track the ocean variability constantly and minimizes its effect on the underwater communication system. In [7], a channel estimate based equalizer was proposed that calculates the filter weights based upon estimates of the time-varying IR of the acoustic channel between the transmitter and receiver and the statistics of the ambient noise field. Although the pTR-based systems compensate for the channel multipath, they are very sensitive to the underwater channel variabilities. In [8], Preisig compared the performance of this channel estimate based decision feedback equalizer and pTR equalizer in the presence of imperfect channel estimates. The results suggested that the performance of this equalizer degrades significantly in the presence of rapid environmental variations, e.g. sea surface variations. In [9], TR approach was combined with adaptive channel equalization to enhance the performance of the communication system. A detailed analysis of several solutions to deal with the ISI in a TR system are presented in [10].

In addition to the time spreading, the received signal also spreads in the frequency domain due to environmental variations (e.g surface variations) and/or geometric variations (e.g source and/or receiver motion). This phenomenon is termed as Doppler spreading. These variations also affect the temporal focusing of the pTR communication system

resulting in the performance loss. In [11], it was shown that a continuous channel update and Doppler tracking are required before TR operation in order to achieve acceptable performance in presence of ocean variability. In a two-part paper [12], [13], a channel tracker was combined with a linear decoder to combat large Doppler spread.

In the multipath environment, the transmitted signal reaches the receiver through different paths where each path is affected by the environmental variations in a different manner, resulting in different amount of Doppler in each path [14]. In the current Doppler compensation techniques, the Doppler distortion is compensated with a single value which fails to give maximum compensation [15], [16]. In [1] an improved version of pTR was proposed, called Frequency Shift Passive Time Reversal (FSpTR) equalizer. FSpTR equalizer was designed to compensate for the source/receiver motion by applying appropriate frequency shifts in the channel IR estimate. Since each path is affected differently by the environmental variations, FSpTR fails to compensate accurately for these channel variabilities which results in residual ISI at the FSpTR system output. In [17] DFE was integrated with FSpTR to improve the performance of the communication system.

In this work, the concept of beamforming is integrated with FSpTR technique to compensate each wavefront separately for the environmental variations. The beamforming technique was applied for underwater communications in [18] where a coherent path beamformer (CPB) was proposed for processing the signals using an adaptive processor that forms a beam in the direction of a collection of coherent signals representing the strongest path. In the direction of interference the processor forms a null beam therefore canceling interference within the principal beam [19], [20]. In [21] CPB is combined with a recursive least-square (RLS) filter to further improve the performance of the system. In CPB, only the strongest path was enhanced and nulls were placed in all the other paths thus ignoring the energy from the other paths which is a disadvantage, while in this work all the paths are compensated separately for their time variability and combined coherently. The paper is organized as follows: Section II will explain the problem statement using a Doppler-based system model. Section III will elaborate the proposed approach of combining FSpTR with the beamformer for adequate Doppler compensation. Section IV will present the complete system diagram. Section V will present underwater communication results from simulated data and real data. Section VI will give the conclusion and some future work.

## II. DOPPLER-BASED SYSTEM MODEL

The objective of this section is to describe the system model adopted in this work and to show how the Doppler affects the transmitted signal. The Doppler effect is usually modeled as a compression/expansion of the transmitted signal and it is shown, in this section, that this effect can be described in terms of time variable IRs.

In underwater transmission systems, the transmitted signal

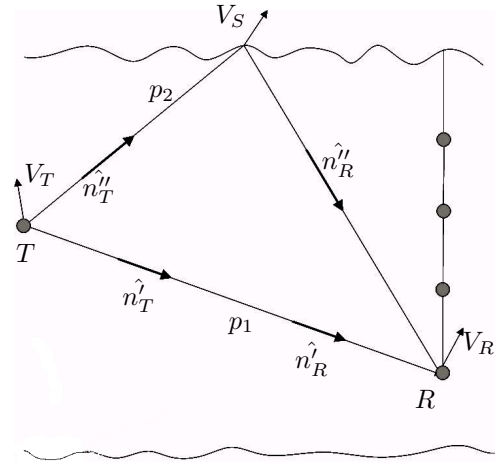


Fig. 1. Two arriving paths from Transmitter to Receiver: Path  $p_1$  is the direct path from the source to the receiver while  $p_2$  is the surface reflected path. In the figure  $V_T$ ,  $V_R$  and  $V_S$  are the velocity vectors at the transmitting, receiving and the surface reflection point respectively.  $\hat{n}'_T$  and  $\hat{n}'_R$  are the unit vectors in the directions of the propagation of the transmitted and received signal for the direct path while  $\hat{n}''_T$  and  $\hat{n}''_R$  are the unit vectors for the surface reflected path.

reaches the hydrophone through different paths which can be categorized as the surface reflected, bottom reflected and water column refracted paths. Figure 1 shows a simplified ray diagram showing two paths  $p_1$  and  $p_2$  from the source  $T$  to the hydrophone  $R$ . Path  $p_1$  is the direct path from the source to the receiver while  $p_2$  is the surface reflected path. Considering only the surface induced motion, path  $p_1$  is affected by the up-down movement of the surface suspended array and range movement of the transmitter, while  $p_2$  is directly affected by the surface motion. The purpose of this analysis is to show that both of these paths are affected by the environmental variations in a different way, resulting in different amounts of Doppler in each path. In figure 1,  $V_T$ ,  $V_R$  and  $V_S$  are the velocity vectors at the transmitting, receiving and the surface reflection points respectively,  $\hat{n}'_T$  and  $\hat{n}'_R$  are the unit vectors in the directions of the propagation of the transmitted and received signal for the direct path and  $\hat{n}''_T$  and  $\hat{n}''_R$  are the unit vectors for the surface reflected path.

The Doppler induced in the received signal, due to these environmental variabilities, is given by [22] which is obtained from the compression/expansion factors

$$s' = \frac{(V_T \cdot \hat{n}'_T - V_R \cdot \hat{n}'_R)/c}{1 - V_T \cdot \hat{n}'_T/c} + 1 \quad (1)$$

for path  $p_1$  and

$$s'' = \frac{((V_T - V_S) \cdot \hat{n}''_T - (V_S - V_R) \cdot \hat{n}''_R)/c}{(1 - V_S \cdot \hat{n}''_R/c)(1 - V_T \cdot \hat{n}''_T/c)} + 1 \quad (2)$$

for path  $p_2$ . In (1) and (2) the sound speed  $c$  is assumed to be constant and  $V_{(\cdot)} \cdot n_{(\cdot)}$  represents the projection of the velocity vectors in the path directions.

In the following, for simplicity, it will be assumed that only the source is moving and that  $v_p$  represents the projection of  $V_T$  in the path direction. In such conditions it was shown in [23] that the base-band Doppler distorted received signal at

the  $i^{th}$  hydrophone of an array for a single propagation path  $p$  is given by the time variable convolution

$$y_{ip}(t) = \int x(t - \tau)[h_{ip}(t, \tau)e^{-j\omega_c\tau}]d\tau \quad (3)$$

where  $\tau$  represents the path delay,  $t$  is the time axis,  $\omega_c$  is the carrier frequency of the band limited transmitted signal  $x(t)$  in base-band and

$$h_{ip}(t, \tau) = \frac{c - v_p}{c} g_{ip}(\tau + (t - \tau)\frac{v_p}{c}) e^{j\omega_c(\tau + (t - \tau)\frac{v_p}{c})} \quad (4)$$

is the time-variable IR in pass-band that results from the Doppler distortion of the initially propagated path  $p$

$$h_{ip}(t = 0, \tau) = g_{ip}(\tau) e^{j\omega_c\tau} \quad (5)$$

In (5),  $g_{ip}(\tau)$  represents a single path,  $p$ , propagating between the source and the receiver, when the signal is assumed to be transmitted at  $t = 0$  and received at the hydrophone after a delay  $\tau$  in a static environment with  $v_p = 0$ . In (4), the path length  $l_p(t)$  changes with a velocity  $v_p = \partial l_p(t)/\partial t$  due to the source motion during the signal transmission. The ratio between this velocity and the sound speed,  $c$ , induces a delay spread in the argument of  $g_{ip}(\tau)$  and a frequency spread in the form complex exponential given in (4). Such frequency variation is responsible for the Doppler spread that also depends on the central frequency,  $\omega_c$ , of the narrowband transmitted signal. Equation (4) gives the time variable IR for a single path which can be generalized to a multipath channel by

$$h_i(t, \tau) = \sum_p h_{ip}(t, \tau_{ip}) \delta(\tau - \tau_{ip}). \quad (6)$$

Performing a time variant convolution, similar to (3), between (6) and the transmitted signal  $x(t)$

$$y_i(t) = \int x(t - \tau)[h_i(t, \tau)e^{-j\omega_c\tau}]d\tau \quad (7)$$

that represent the Doppler distorted signal received by the  $i^{th}$  hydrophone in a multipath channel.

Assuming a plane wave approximation, it can be shown that the Frequency Responses (FRs) of the time-variable IRs of a VLA, given by (6), can be computed as

$$H_i(t, \omega) = \sum_p e^{-j\omega\tau_{ip}} [e^{j\omega t \frac{v_p}{c - v_p}} G_p(\frac{c}{c - v_p}\omega - \omega_c)] \quad (8)$$

that results from the Doppler distortion of the channel FRs when  $t = 0$  and  $v_p = 0$  which is given by

$$H_i(t = 0, \omega) = \sum_p e^{-j\omega\tau_{ip}} G_p(\omega - \omega_c) \quad (9)$$

In (8) and (9), due to the plane wave approximation, it was considered that  $G_{ip}(\cdot) \approx G_p(\cdot)$ .

In (8) the term in  $[\cdot]$  represents the time dependent Doppler distortion experienced by path  $p$  at hydrophone  $i$  in the frequency domain. The first complex exponential represents the delay encountered by each path, that in the plane wave assumption is given by  $\tau_{ip} = \tau_p - \Delta_i$  where  $\tau_p$  represents the delay from the source to a reference hydrophone of the VLA and  $\Delta_i$  is the wavefront delay between the  $i^{th}$  and the

reference hydrophones.

In (8), due to the plane wave approximation, the velocity  $v_p$  experienced by all the paths of a given wavefront is always the same which means that the Doppler distortion is constant for each wavefront that arrives to the VLA. That is more valid when the environmental variability is due to the source motion or when all hydrophones, of the VLA, experience the same motion. However when the environmental variabilities for the paths in a wavefront are different, as is the case of surface wave motion, this is only approximately true.

### III. THE BF-FSpTR DOPPLER COMPENSATION

This section will present the Beamforming Frequency Shift passive Time Reversal (BF-FSpTR) Doppler compensation system. The proposed BF-FSpTR system will be developed considering that the transmitted signal is a Dirac impulse and in section IV it will be extended for communication signals. The BF-FSpTR system is based on the pTR operator, also termed as Passive phase conjugation in the frequency domain [24], that is able to deconvolve the channel multipath for time invariant channels. The phase conjugation (PC) operation is given by

$$P_{PC}(t, \omega) = \sum_i H_i^*(t = 0, \omega) H_i(t, \omega) \quad (10)$$

where  $*$  denotes conjugate operation,  $H_i(t = 0, \omega)$  is the initial FR estimate for the  $i^{th}$  hydrophone of the VLA and  $H_i(t, \omega)$  is the corresponding Doppler distorted FR.

Considering that  $H_i(t, \omega)$  and  $H_i^*(t = 0, \omega)$  are given by (8) and (9) respectively and there is no channel variability ( $v_p = 0$ ) (which is equivalent to no Doppler distortion) the PC operator in (10) becomes

$$\begin{aligned} P_{PC, v_p=0}(t, \omega) &= \sum_i \sum_p e^{-j\omega\tau_{ip}} G_p^*(\omega - \omega_c) \\ &\quad \sum_p e^{j\omega\tau_{ip}} G_p(\omega - \omega_c) \\ &= I \sum_p |G_p(\omega - \omega_c)|^2 \end{aligned} \quad (11)$$

In (11) all paths are summed coherently which result in a channel with an enhanced single propagation path.

In the presence of environmental variability, with  $v_p \neq 0$  the PC operator will be affected by Doppler and (10) becomes

$$P_{PC, v_p \neq 0}(t, \omega) = \sum_p [G_p^*(\omega - \omega_c) G_p(\frac{c}{c - v_p}\omega - \omega_c)] e^{j\omega t \frac{v_p}{c - v_p}} \quad (12)$$

In (12) the paths can no longer be summed coherently and the product in  $[\cdot]$  would not result in a flat FR since the arguments of  $G$ 's are different. In such case the multipath is only partially compensated when  $v_p \approx 0$ , that is in presence of small Doppler distortion.

In [1] the FSpTR was presented and it was shown, in the normal mode context, that the channel variability of (12) can be partially compensated by applying an appropriate frequency shift to the initial FR estimate,  $H_i^*(t = 0, \omega)$ , of (10). In such

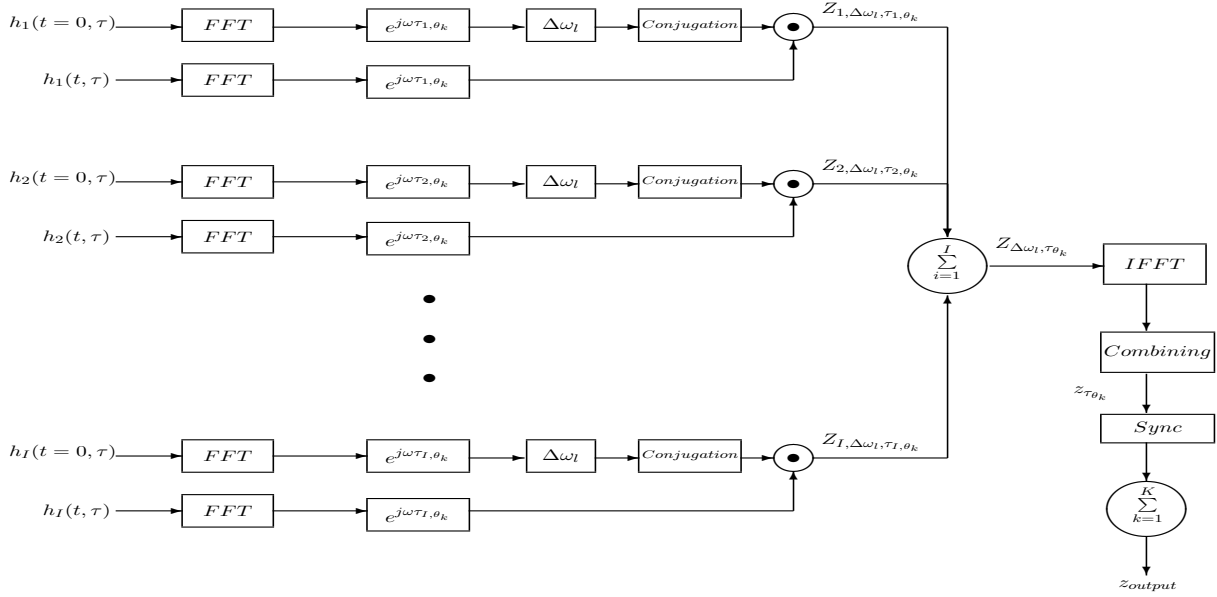


Fig. 2. Block Diagram of the BF-FSpTR system

conditions (10) becomes

$$P_{PC, v_p \neq 0, \Delta\omega}(t, \omega) = \sum_p e^{j\omega t \frac{v_p}{c-v_p}} \sum_i e^{j\tau_{ip} \Delta\omega} [G_p^*(\omega - \Delta\omega - \omega_c) G_p(\frac{c}{c-v_p} \omega - \omega_c)] \quad (13)$$

where  $\Delta\omega = -\omega_c \Delta\omega'$  is the applied frequency shift. Putting  $\Delta\omega' = \frac{v_p}{c-v_p}$  partially compensates the term in  $[\cdot]$  since for a narrow band signal

$$\omega \frac{c}{c-v_p} = \omega + \omega \frac{v_p}{c-v_p} \approx \omega + \omega_c \frac{v_p}{c-v_p} \quad (14)$$

The exponential term will not be discussed here since this is not the purpose of the paper. Since the optimum frequency shift  $\Delta\omega$  is not known a-priori in the FSpTR processing, a set of  $L$  frequency shifts are applied and the one that gives the maximum power of (13) is selected. The FSpTR technique can apply a single frequency shift which can only compensate for the variability of a single wavefront or a group of wavefronts that arrives to the VLA at similar angles.

The BF-FSpTR was developed to overcome the FSpTR problem of compensating a limited number of wavefronts. It adds an angular dimension to the Doppler distorted and initial estimated FRs in (8) and (9) respectively, which results in

$$H_{i\theta}(t, \omega) = \sum_p e^{-j\omega\tau_{ip}} e^{j\omega\tau_{i\theta}} [e^{j\omega t \frac{v_p}{c-v_p}} G_p(\frac{c}{c-v_p} \omega - \omega_c)] \quad (15)$$

$$H_{i\theta}(t=0, \omega) = \sum_p e^{-j\omega\tau_{ip}} e^{j\omega\tau_{i\theta}} G_p(\omega - \omega_c) \quad (16)$$

where  $\tau_{i\theta} = \frac{d_i}{c} \sin \theta_k$  corresponds to the time delay step of the beamformer,  $\theta_k$  is the corresponding angle of observation,  $d_i$  is the spacing between the  $i^{th}$  and the reference hydrophone of the VLA and  $c$  is the sound speed between the corresponding hydrophones. After applying the PC operation with (15) and

(16) it results

$$P_{PC, v_p \neq 0, \Delta\omega, \theta}(t, \omega) = \sum_p e^{j\omega t \frac{v_p}{c-v_p}} e^{j\tau_p \Delta\omega} \sum_i \{e^{j\Delta_i \Delta\omega} e^{j\tau_{i\theta} \Delta\omega}\} [G_p^*(\omega - \Delta\omega - \omega_c) G_p(\frac{c}{c-v_p} \omega - \omega_c)] \quad (17)$$

where the complex exponential product in  $\{\cdot\}$  is unity when  $\Delta_i = \tau_{i\theta}$ , thus implementing a beamformer in the frequency shift domain. In (17) a different frequency shift can be applied for each angle of observation,  $\theta_k$ , which is equivalent to compensating each wavefront with a different frequency shift. In (17) the two exponentials

$$e^{j\tau_p \Delta\omega}$$

and

$$e^{j\omega t \frac{v_p}{c-v_p}}$$

represents a phase shift and a phase rotation that are left uncompensated.

Figure 2 shows the block diagram of the current implementation of the BF-FSpTR. In the block diagram  $Z_{\Delta\omega_l, \tau_{l, \theta_k}} \equiv P_{PC, v_p \neq 0, \Delta\omega, \theta}(t, \omega)$  and reveals that in the BF-FSpTR current implementation, a set of frequency shifts  $\Delta\omega \equiv \Delta\omega_l$  and a set of angles of observation  $\theta \equiv \theta_k$  are applied discretely. The optimum frequency shift for the compensation of each angle of observation is selected in the "Combining" block by selecting the  $\Delta\omega_l$  that gives the maximum output power for each angle. The "Sync" block compensates for the exponentials that were left uncompensated in (17). The synchronization operation will be discussed in detail in section IV. After the sync block, the outputs  $z_{\tau_{\theta_k}}$  for all angle of observation,  $\theta_k$  are summed coherently resulting in  $z_{output}$  which should be a Dirac impulse when the BF-FSpTR compensation mechanism operates appropriately.

Figures 3 to 5 illustrate the behavior of the BF-FSpTR system.

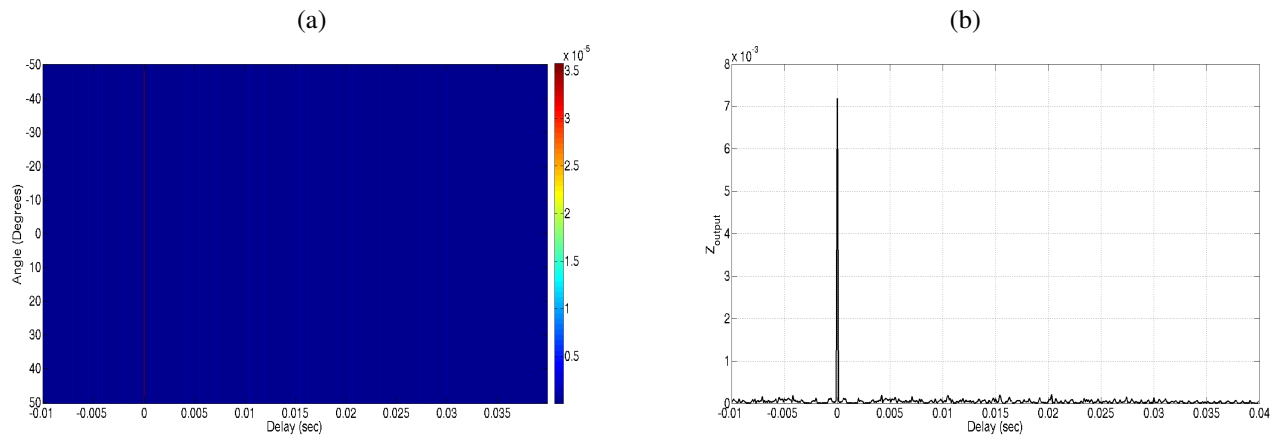


Fig. 3. (a) Output of the combining block in figure 2 considering no frequency shift and identical IRs: (a) angle delay-spread plane, (b) sum over the angles,  $Z_{output}$

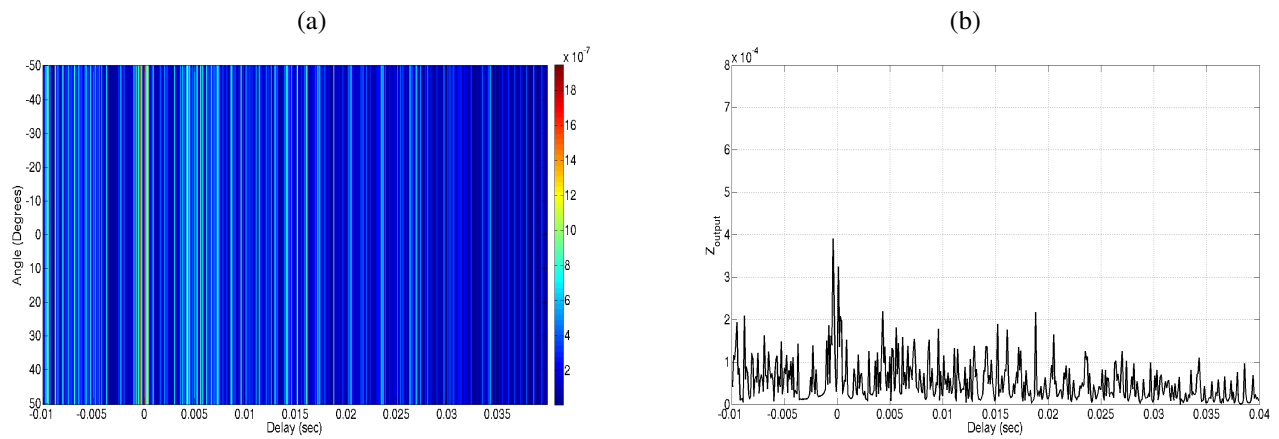


Fig. 4. (a) Output of the combining block in figure 2 with no frequency shift and using mismatched IRs: (a) angle delay-spread plane, (b) sum over the angles,  $Z_{output}$

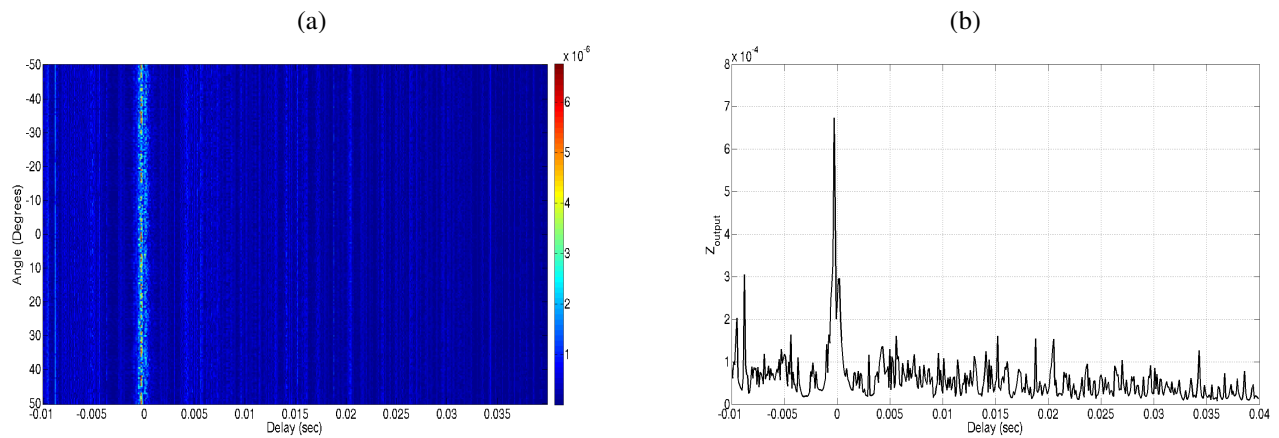


Fig. 5. (a) Output of the combining block in figure 2 with optimal frequency shift compensation and using mismatched IRs: (a) angle delay-spread plane, (b) sum over the angles,  $Z_{output}$

In these three different simulated scenarios (further described in section V-A), (a) represents the output IR observed for each angle,  $z_{\tau\theta_k}$ , and (b) shows the output after the summation over all angles,  $z_{output}$ . In all cases the initial-field,  $h(t = 0, \tau)$ , is the one shown in figure 8 (a). In case (i), depicted in figure 3, there is no mismatch and  $h(t = 0, \tau) \equiv h(t, \tau)$ ; in case (ii), shown in figure 4, there is a mismatch between the initial-field and the mismatch-field  $h(t, \tau)$ , thus  $h(t = 0, \tau) \neq h(t, \tau)$  but the combining block does not compensate for the channel mismatch and selects 0 Hz as the frequency shift. In figure 5, the same initial-field and the mismatch-field of case (ii) are being used, but now the combining block selects the optimal frequency,  $\Delta\omega_l$ , for each angle  $\theta_k$ , depending on the maximum output power.

Figure 3 (a) shows that the field is almost constant for all angles with a single arrival at lag zero, which means that there is a focus in time and space. Figure 3 (b) shows that, after the summation over all angles, the overall IR becomes a Dirac impulse. Figure 4 shows that the mismatch between the initial-field and the mismatch-field is not compensated by applying the frequency shift, thus there are multiple arrivals with different delays which constitutes to the inter-Symbolic Interference (ISI) in communications context. Figure 4 (b) shows an overall IR with strong multipath effect. The main focusing peak is masked by the ISI resulting in low amplitude and the main peak is at 0 sec. Figure 5 (a) shows that when the frequency shift attempts to compensate for the channel mismatch there is a strong concentration of energy around 0 sec but it is not uniform over all angles. Figure 5 (b) reveals that the frequency compensation results in a strong multipath reduction and that the BF-FSpTR provides a partial compensation for the channel mismatch.

For underwater communication applications, the overall IRs observed in Figures 3 to 5 reveal that ISI would be almost zero when there is no mismatch between  $h(t = 0, \tau)$  and  $h(t, \tau)$  while in case of channel mismatch, the ISI would be quite large. Finally, due to the frequency shift compensation there is a strong reduction in ISI, which will improve the performance of a communication system.

#### IV. THE BF-FSpTR COMMUNICATION SYSTEM

Figure 6 shows the block diagram of the BF-FSpTR system when applied to underwater communications. The implementation of BF-FSpTR was explained in section III using the channel IRs at different time instants. For the propose of applying the BF-FSpTR for data communications, the channel IR  $h_i(t, \tau)$  is replaced by the data signal denoted by  $q'_i$  which should contain the information data sequence convolved with  $h_i(t, \tau)$ .

The proposed block diagram is shown in figure 6, where conceptually in the upper part of the diagram, the transmitted pulse  $\delta(t)$  is passed through the channel  $h_i(t)$  that represent the channel IRs during probe transmission, at hydrophone  $i$  of the VLA, further added with additive white Gaussian noise (AWGN),  $u(t)$ , resulting that  $q_i(t) = h_i(t) + u_i(t)$ . In the lower part of the block diagram the data signal  $a(n)$  is pulse shaped by a root raised cosine signal and convolved with the

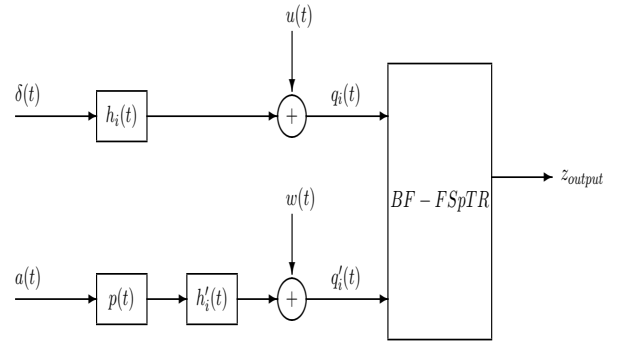


Fig. 6. block diagram of the BF-FSpTR system, applied to underwater communications

channel IRs,  $h'_i$ , that represents the channel during the signal transmission. The noise  $w(t)$  is added to the resulting signal to get  $q'_i(t)$  and then fed to the BF-FSpTR block. In order to apply the FSpTR frequency shift compensation, the channel IRs are assumed to be almost constant (frozen) during 0.25 second and  $q'_i$  is divided in slot of 0.25 second before being applied to the BF-FSpTR block [1].

The output of the BF-FSpTR block,  $z_{output}$ , will be the data,  $a_n$ , convolved with an overall IR similar to the one shown in figure 5 (b), as discussed in section III. Similarly  $z_{output}$  is also divided in slots of 0.25 second duration and the frequency shift channel-variability compensation, provided by the FSpTR, is not applied to the instantaneous channel but to the channel-variability during the correspondent 0.25 second, which is assumed to be negligible.

An important implementation issue of this system is to synchronize the uncompensated exponentials in all Doppler compensated data signals corresponding to each angle of observation,  $\theta_k$ , of the beamformer, as shown in (17). Each data signal is affected by the environmental variations in a different manner and different frequency shifts compensate for these variations for each angle, resulting in different phase shifts for each data signal. By summing these data signals, to obtain  $z_{output}$ , the desired performance is not achieved due to non-coherent summation. The *sync* block synchronizes each data signal with a known M-sequence which is transmitted every second in the transmitted data signal.

Another important parameter which affects the performance of the BF-FSpTR is the angular range. The angular range is the set of angles used to search for different wavefronts. Figure 8 (b) shows the beamforming results of the simulated scenario (further described in section V-A), where it can be seen that for an angular range of -10 to 10 degrees only two wavefronts would be compensated, and if the angular range is increased to -50 to 50 degrees, all 6 wavefronts would be considered. The angular range of the system must be such that it incorporates all the arrivals reaching the receiver. Nevertheless the BF-FSpTR results have shown that even a smaller range of angles gives better performance than FSpTR as it compensates for each arrival separately.

## V. PERFORMANCE COMPARISON OF pTR, FSpTR AND BF-FSpTR

This section elaborates the performance comparison of the proposed system with the FSpTR and pTR systems. In order to show the effectiveness of BF-FSpTR, simulated as well as real data results are presented in this section. In the first part of this section two simulated scenarios are presented in which the performance of BF-FSpTR is compared with FSpTR and pTR. In the last part of this section real data results are also presented.

### A. Simulated Data Scenarios

In order to simulate the underwater environment, the Time Variable Acoustic Propagation Model (TV-APM) [23] is used. Two cases will be considered with a source-receiver range of 1 km and a source depth of 12 m. A 16 hydrophones VLA is considered with the first hydrophone placed at 6 m depth and an inter spacing between the hydrophones of 4 m. A flat surface is considered in TV-APM and figure 7 shows the sound speed profile (SSP) used in TV-APM for both cases.

In the first case, the source is considered to be moving only along the vertical direction with the velocity of 0.5 m/s. Figure 8 (a) shows the initial arriving pattern of the channel. It can be seen that there are six wavefronts arriving at the VLA, with the first two arrivals superimposed for the top hydrophones. Figure 8 (b) shows the beamformer result where all the six wavefronts can be seen in the angle delay-spread plane. The negative angles show the wavefronts from the bottom while the positive angles show the wavefronts from the surface.

Figure 9 (a) shows the Doppler spectrum of the channel at hydrophone 6 which is placed at 26 m depth. The source is moving in the vertical direction, but different values of Doppler are induced in each arrival, a small value for the initial arrivals while a relatively bigger values for the latter arrivals. This observation shows that each arrival is affected differently by the same environmental variation and that a single frequency shift will not be enough to compensate for all these variations.

The second case also has the same geometry but now the source is considered moving in both horizontal and vertical directions with a velocity of 0.5 m/s. The initial arriving pattern of the channel and the corresponding beamformer are the same as for the first case which is shown in figure 8. Figure 9 (b) shows the Doppler spectrum at hydrophone 6, which is placed at 26 m depth, for the second case. Due to the simultaneous movement along horizontal and vertical directions, higher values of Doppler are induced in all arrivals.

### B. Simulated Data Results

This subsection elaborates the performance comparison of pTR, FSpTR and BF-FSpTR in terms of MSE. The data set used for the analysis has a bit rate of 2000 bits/sec, a carrier frequency of 10000 Hz and BPSK as the modulation scheme. Figure 10 (a) shows the performance comparison in terms of MSE for case (i) when the BF-FSpTR angular range is -10 to

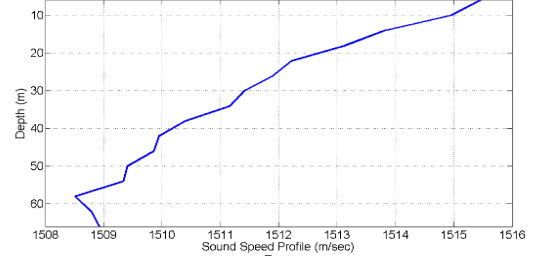


Fig. 7. downward refracting sound speed profile.

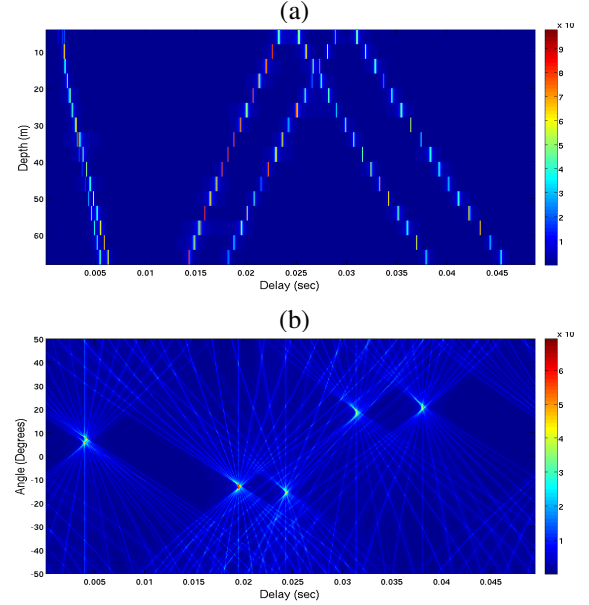


Fig. 8. simulated channel characterization: a) channel IR estimates b) the beamforming result showing the angle of arrival of different arrivals taking hydrophone 8 as the reference hydrophone, so the delay axis is representing the delay for each wavefront w.r.t hydrophone 8.

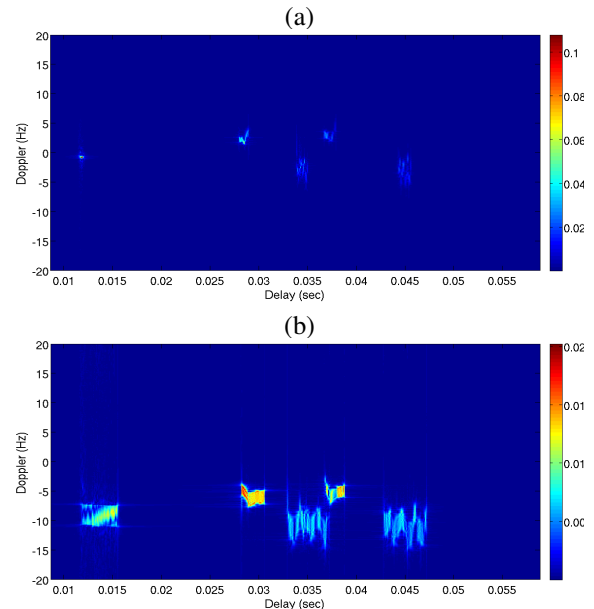


Fig. 9. Doppler spread, at hydrophone 6 placed at 26 m depth, due to a) source vertical motion of 0.5 m/s, b) source vertical and horizontal motion of 0.5 m/s

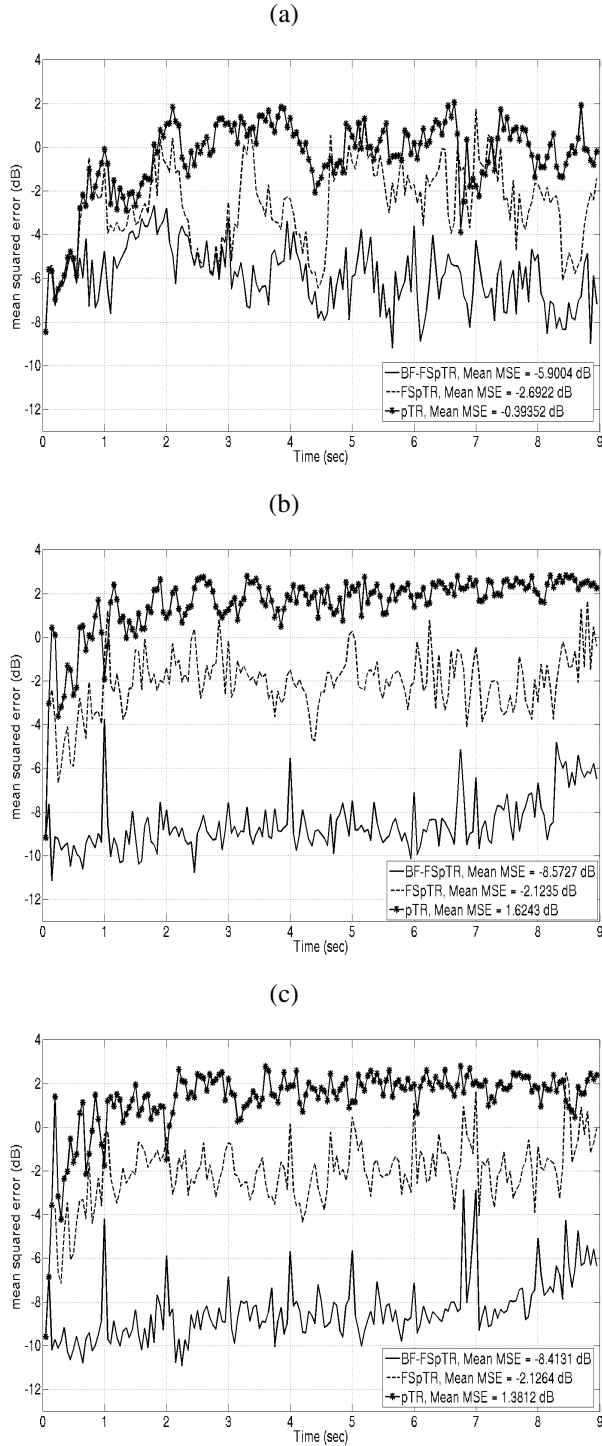


Fig. 10. Case (i); MSE performance of pTR, FSpTR and BF-FSpTR, (a) considering an angular range of -10 to +10 degrees, (b) considering an angular range of -50 to +50 degrees. (c) Case (ii); MSE performance of pTR, FSpTR and BF-FSpTR considering an angular range of of -50 to +50 degrees.

+10 degrees which means that the variability of the first two arrivals can be compensated. In order to make the comparison between pTR, FSpTR and BF-FSpTR in similar conditions, only the initial two arrivals were used as IR estimate for the computation of pTR and FSpTR, since only these two arrivals reach the receiver between -10 to 10 degrees (see

figure 8). Figure 10 (a) shows that the performance of BF-FSpTR is better than pTR and FSpTR during the whole 9 sec with a mean MSE gain of 5.5 dB and 3.3 dB for pTR and FSpTR respectively. It should be noted that the performance of all the three systems is identical at the starting point as the initial IR estimate replicates accurately the channel during data transmission. With the passage of time, the performance of pTR degrades severely due to the geometric variation (source motion) which results in loss in temporal focusing. The FSpTR system tries to compensate for these variations by applying a single frequency shift for the first two arrivals in the estimated channel IR which results in an improvement of 2.3 dB in mean MSE.

Figure 10 (b) shows the results of the same case but with the angular range of the BF-FSpTR increased to -50 to +50 degrees and all six wavefronts considered in the pTR and FSpTR IR estimate window. The performance of the three systems is identical in the beginning but in this case, for pTR and FSpTR, the performance degrades suddenly from the start. The mean MSE values of -2.12 dB and +1.62 dB is achieved for the whole 9 sec for pTR and FSpTR respectively, while the performance of BF-FSpTR remains almost the same for the whole 9 sec with the mean MSE value of -8.57 dB. The MSE performance degradation of pTR can be explained by the fact that the IR mismatch increases by increasing the number of uncompensated arrivals. Similarly, the performance of FSpTR also degrades as a single frequency shift fails to compensate for the environmental variations experienced by all the arrivals. On the other hand, the BF-FSpTR compensates all the arrivals with different frequency shifts and thus the performance improves. Comparing figure 10 (a) and (b) it can be observed that by increasing the angular range the BF-FSpTR mean gain in MSE increases by 2.6 dB.

Figure 10 (c) shows the MSE performance comparison for case (ii) between pTR, FSpTR and BF-FSpTR, for the angular range of -50 to 50 degrees. It can be seen that BF-FSpTR gives a mean MSE gain of 9.79 dB and 6.29 dB for pTR and FSpTR respectively. Comparing the system performances with the previous simulated scenarios, it can be observed that BF-FSpTR can compensate for the Doppler induced by the vertical and horizontal motion of the source in a more efficient manner.

### C. Real data scenario

The data set, shown in this section, was collected during the UAB'07 experiment. During the experiment the source was suspended by a crane from a fixed platform, 10 m from shore, at an initial depth of 5 m. The receiver was a surface suspended VLA with 16 hydrophones uniformly spaced at 4 m between 6 m to 66 m depth. The communication range was approximately 1 km with the water column depth of 12 m at source location and about 120 m at array location. A more detailed description of the experiment can be found in [25].

Figure 11 (a) shows the initial IR estimate where it can be seen that a large number of arrivals are reaching the receiver with different delays. Figure 11 (b) shows the angle of arrival

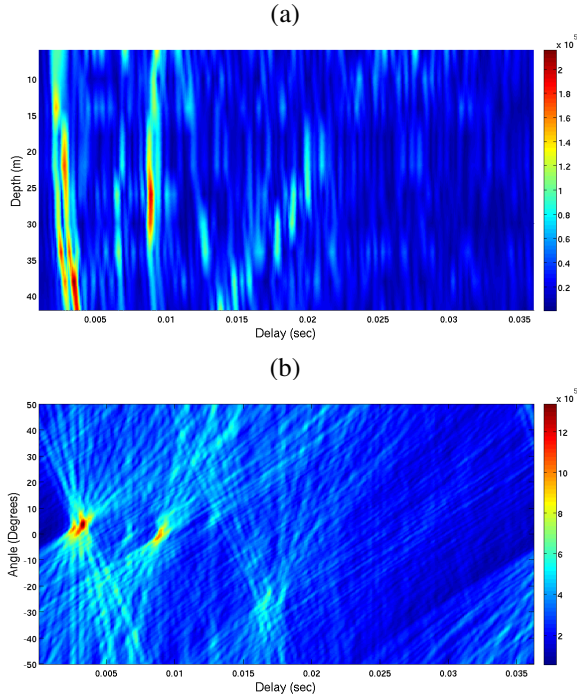


Fig. 11. a) channel IR estimates of the real dataset, b) The Beamforming result showing the angle of arrival of different arrivals

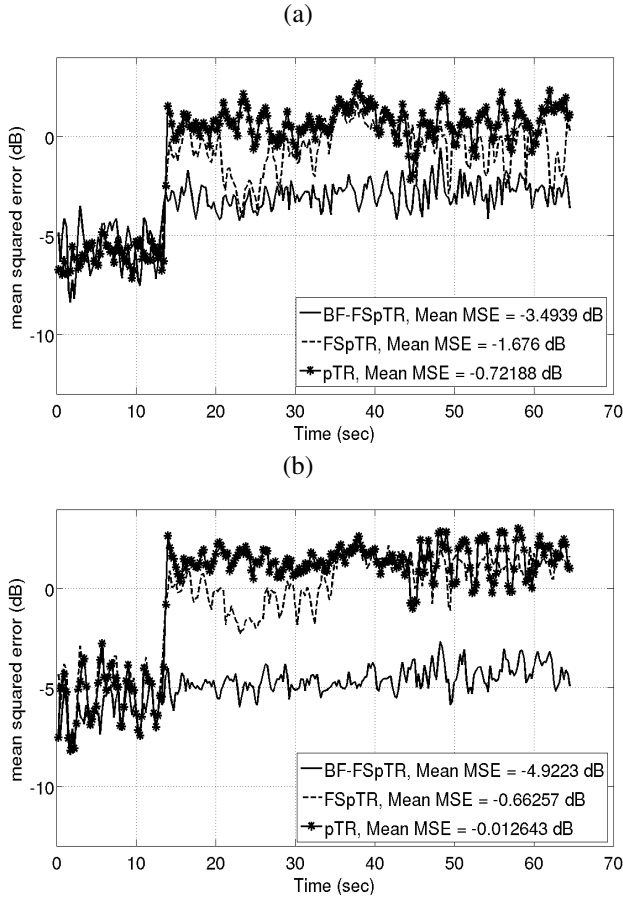


Fig. 12. real data MSE performance comparison between pTR, FSpTR and BF-FSpTR, (a) considering an angular range of -10 to +10 degrees, (b) considering an angular range of -50 to +50 degrees.

of different wavefronts. It can be seen that there are two strong arrivals at approximately 3 degree and the third and fourth arrival at approximately 0 degree. Also there is another strong arrival at approximately -30 degree. In the arriving pattern, shown in figure 11 (a), the later arrivals are very unstructured and it is very difficult to differentiate between different wavefronts. In the arriving pattern, there is an arrival at approximately 0.01 sec (the one at 0°) which is almost vertical which means that it arrives at all hydrophone at the same time. This is an abnormal behavior for a later arrival as these arrivals are usually bottom or surface reflected and they reach all the hydrophones of the array with different delays. The probable reason for this behavior is that there may be a tilt in the hydrophone array due to the currents and thus all the hydrophones received the wavefront at almost the same time.

#### D. Real Data Results

The transmitted signal, presented in this section, comprised of 50 chirp signals followed by a data set of 100 seconds. The chirp transmission was used for the channel IR estimation and to study the channel variability and Doppler spread. Each chirp had a bandwidth of 2.5 kHz ranging from 5 to 7.5 kHz with 0.1 sec duration whereas data bandwidth ranges from 5.5 to 7 kHz with BPSK modulation and baud rate of 1000 bits/sec. A carrier frequency of 6250 Hz was used.

Figure 12 (a) shows the performance of BF-FSpTR for an angular range of -10 to +10 degrees. Comparing the performance of pTR, FSpTR and BF-FSpTR in figure 12 (a) it can be seen that BF-FSpTR outperforms FSpTR and pTR and there is a mean MSE gain of 1.8 dB and 2.8 dB respectively.

Figure 12 (b) shows the performance in the same data set but the angular range is increased to -50 to +50 degrees and the improvement in the performance is clearly visible. The MSE performance of BF-FSpTR improves resulting in a mean gain in MSE of 4.9 dB. On the other hand the performance of pTR and FSpTR degrades by 1 dB and 0.7 dB respectively, which is due to the increase in the size of IR window. The effect of increasing the angular range can also be seen from the beamforming result in figure 11 where it is clearly visible that there are four arrivals between -10 to 10 degrees and there is another arrival at approximately -30 degrees. By increasing the angular range all the arrivals are included and compensated by the BF-FSpTR, thus improves the performance of the system.

## VI. CONCLUSION AND FUTURE WORK

In this paper a new signal processing technique called Beamformed FSpTR (BF-FSpTR) is presented. BF-FSpTR is an arrival-based approach which isolates different arrivals in the multipath environment and compensates for each arrival separately as each arrival is affected in a different way by the environmental variations resulting in different amount of Doppler.

The performance comparison of BF-FSpTR approach with pTR and FSpTR is presented. In this paper, BF-FSpTR is tested with two simulated data sets and one real data set

collected during the UAB'07 experiment. Among the two simulated data sets the source is considered moving only in the vertical direction with a velocity of 0.5 m/s in the first case and in the second case the source is considered moving both in horizontal and vertical directions with a velocity of 0.5 m/s. The results showed that BF-FSpTR outperforms pTR and FSpTR. In the first case, there is a mean MSE gain of 10.19 dB and 6.45 dB as compared to pTR and FSpTR respectively, while in the second case mean MSE gains of 9.79 dB and 6.29 dB are achieved. In case of real data, BF-FSpTR compensated for the environmental variations more effectively resulting in a mean MSE gain of 4.9 and 4.2 dB as compared to pTR and FSpTR respectively.

The effect of angular range of the beamformer is also studied in this work. It is observed that by increasing the angular range the performance of BF-FSpTR is improved which is due to the fact that by increasing the angular range, more arrivals are included and BF-FSpTR compensates for each of them separately by applying appropriate frequency shift resulting in higher gain in terms of MSE.

The work presented in this paper includes some preliminary observations and results of the BF-FSpTR system. These results have shown that BF-FSpTR has the potential of improving the performance of the underwater communication system. BF-FSpTR is an open field of research so different issues should be addressed in future work to understand the behavior of the BF-FSpTR system in more detail.

#### ACKNOWLEDGEMENTS

This work is supported by Portuguese Foundation for Science Technology under PHITOM (PTDC/EEA-TEL/71263/2006) and COGNAT (PTDC/MAR/112446/2009) projects. This work was also supported by European Community's Sixth Framework Program through the grant to the budget of the Integrated Infrastructure Initiative HYDRALAB III within the Transnational Access Activities, Contract no. 022441.

#### REFERENCES

- [1] A. Silva, S.M. Jesus, and J. Gomes. Environmental equalizer for underwater communications. In *OCEANS 2007*, pages 1–7, 29 Oct–4 Nov 2007.
- [2] W. A. Kuperman, William S. Hodgkiss, Hee Chun Song, T. Akal, C. Ferla, and Darrell R. Jackson. Phase conjugation in the ocean: Experimental demonstration of an acoustic time-reversal mirror. *The Journal of the Acoustical Society of America*, 103(1):25–40, 1998.
- [3] J. S. Kim, H. C. Song, and W. A. Kuperman. Adaptive time-reversal mirror. *The Journal of the Acoustical Society of America*, 109(5):1817–1825, 2001.
- [4] G.F. Edelmann, W.S. Hodgkiss, S. Kim, W.A. Kuperman, H.C. Song, and T. Akal. Underwater acoustic communication using time reversal. In *OCEANS, 2001. MTS/IEEE Conference and Exhibition*, volume 4, pages 2231–2235 vol.4, 2001.
- [5] M. Stojanovic, J. Catipovic, and J. G. Proakis. Reduced-complexity multi-channel processing of underwater acoustic communication signals. *J. Acoust. Soc. Am.*, 98:961–972, 1995.
- [6] Daniel Rouseff. Intersymbol interference in underwater acoustic communications using time-reversal signal processing. *The Journal of the Acoustical Society of America*, 117(2):780–788, 2005.
- [7] M. Stojanovic; L. Freitag; and M. Johnson. Channel-estimation-based adaptive equalization of underwater acoustic signals. In *OCEANS 1999 MTS/IEEE Conference and Exhibition, Seattle, USA*, pages 985–990, Sept. 1999.
- [8] James C. Preisig. Performance analysis of adaptive equalization for coherent acoustic communications in the time-varying ocean environment. *The Journal of the Acoustical Society of America*, 118(1):263–278, 2005.
- [9] H. C. Song, W. S. Hodgkiss, W. A. Kuperman, Stevenson M., and T. Akal. Improvement of time-reversal communications using adaptive channel equalizers. *Oceanic Engineering, IEEE Journal of*, 31(2):487–496, April 2006.
- [10] Milica Stojanovic. Retrofocusing techniques for high rate acoustic communications. *The Journal of the Acoustical Society of America*, 117(3):1173–1185, 2005.
- [11] Aijun Song, Mohsen Badiiey, H. C. Song, William S. Hodgkiss, Michael B. Porter, and the KauaiEx Group. Impact of ocean variability on coherent underwater acoustic communications during the kauai experiment (kauaex). *The Journal of the Acoustical Society of America*, 123(2):856–865, 2008.
- [12] T. H. Eggen, A. B. Baggeroer, and J. C. Preisig. Communication over doppler spread channels. part i: Channel and receiver presentation. *Oceanic Engineering, IEEE Journal of*, 25:62–71, 2000.
- [13] T. H. Eggen, J. C. Preisig, and A. B. Baggeroer. Communication over doppler spread channels. ii. receiver characterization and practical results. *Oceanic Engineering, IEEE Journal of*, 26:612–621, 2001.
- [14] S. Ijaz, A.J. Silva, O.C. Rodriguez, and S.M. Jesus. Doppler domain decomposition of the underwater acoustic channel response. In *OCEANS 2011 IEEE Conference, Santandar, Spain*, pages 1–7, June 2011.
- [15] Joao Gomes, Antonio Silva, and Sergio Jesus. Adaptive spatial combining for passive time-reversed communications. *The Journal of the Acoustical Society of America*, 124(2):1038–1053, 2008.
- [16] B. S. Sharif, J. Neasham, O. R. Hinton, and Adams A. E. A computationally efficient doppler compensation system for underwater acoustic communications. *Oceanic Engineering, IEEE Journal of*, 25:52–61, 2000.
- [17] U. Vilaipornsawai, A.J. Silva, and S.M. Jesus. Underwater communications for moving source using geometry-adapted time reversal and dfe: Uan10 data. In *OCEANS 2011 IEEE Conference, Santandar, Spain*, pages 1–7, June 2011.
- [18] L. R. LeBlanc and P. P. Beaujean. Underwater communication in shallow water. *Oceanology* 98, Brighton, UK, 2:209–221, 1998.
- [19] L. LeBlanc. Angular-spectral decomposition beamforming for acoustic arrays. *Oceanic Engineering, IEEE Journal of*, 9(1):31–39, jan 1984.
- [20] Lester R. LeBlanc and John I. Salisbury. High resolution wavenumber-frequency methods for towed arrays. *The Journal of the Acoustical Society of America*, 90(6):3155–3160, 1991.
- [21] P.-P.J. Beaujean and L.R. LeBlanc. Spatio-temporal processing of coherent communications data in shallow water. In *OCEANS 2000 MTS/IEEE Conference and Exhibition*, volume 3, pages 1625–1631 vol.3, 2000.
- [22] Lawrence. J. Ziomek. *Fundamentals of Acoustic Field Theory and Space-Time Signal Processing*. CRC, Boca Raton, FL., 1995.
- [23] A. Silva, O. Rodriguez, F. Zabel, J. Huilery, and S. M. Jesus. Underwater acoustics simulations with time variable acoustics propagation model. *Proceeding of 10th European Conference on Underwater Acoustics*, 2:989–996, July, 2010.
- [24] Darrell R. Jackson and David R. Dowling. Phase conjugation in underwater acoustics. *The Journal of the Acoustical Society of America*, 89(1):171–181, 1991.
- [25] S. Ijaz, A.J. Silva, and S.M. Jesus. Compensating for source depth change and observing surface waves using underwater communication signals. In *Fourth International Conference on Sensor Technologies and Applications (SENSORCOMM), 2010*, pages 462–467, July 2010.